

A HEMT-Based Cryogenic Charge Amplifier with sub-100 eVee Ionization Resolution for Massive Semiconductor Dark Matter Detectors

A. Phipps^{a,*}, A. Juillard^b, B. Sadoulet^c, B. Serfass^c, Y. Jin^d

^aDepartment of Physics, Stanford University, Stanford, CA 94305, USA

^bUniversité de Lyon, Université Lyon 1, CNRS/IN2P3, IPN-Lyon, F-69622 Villeurbanne Cedex, France

^cDepartment of Physics, University of California, Berkeley, CA 94720, USA

^dC2N, CNRS, Univ. Paris-Sud, Univ. Paris-Saclay, 91460 Marcoussis, France

Abstract

We present the design and noise performance of a fully cryogenic (T=4 K) HEMT-based charge amplifier for readout of massive semiconductor dark matter detectors operating at sub-Kelvin temperatures. The amplifier has been developed to allow direct detection experiments such as CDMS and EDELWEISS to probe WIMP masses below 10 GeV/c² while retaining electromagnetic background discrimination. The amplifier dissipates only 1 mW of power and has a measured noise performance three times better than traditional JFET-based charge amplifiers. The predicted ionization energy resolution using the measured intrinsic amplifier noises and typical detector characteristics is $\sigma_E \approx 100 \text{ eV}_{ee}$ (33 electrons). We have measured a calibrated baseline energy resolution of $\sigma_E = 91 \text{ eV}_{ee}$ when coupled to a live CDMS-II detector. To our knowledge, this is the best resolution achieved on such massive ($\approx 150 \text{ pF}$ capacitance) radiation detectors.

Keywords: HEMT amplifiers; charge amplifiers; dark matter detectors; analog electronic circuits; front-end electronics

1. Introduction

The Cryogenic Dark Matter Search (CDMS) [1, 2, 3, 4] and EDELWEISS [5, 6, 7, 8] experiments have been setting competitive direct detection dark matter limits using semiconductor radiation detectors operating at sub-Kelvin temperatures for over a decade. These high purity germanium detectors have the ability to distinguish between electromagnetic background and nuclear recoil events caused by Weakly Interacting Massive Particles (WIMPs) through the simultaneous measurement of ionization and phonons produced by an interacting particle. Recently, there has been growing interest in searching for low-mass ($\lesssim 10 \text{ GeV}/c^2$) WIMPs [9, 10, 11, 12] driving the need to develop extremely low noise charge amplifiers for ionization readout due to the lower recoil energy deposited in the detector by an interacting low-mass particle.

The low-mass WIMP detection threshold directly depends upon the baseline detector energy resolution, generally determined by electronic noise in the ionization readout circuit. The circuit integrates the drift current produced by an interacting particle and requires a high impedance input stage with a capacitance well-matched to the detector capacitance of $C_{det} \approx 150 \text{ pF}$ to maximize the signal-to-noise. CDMS and EDELWEISS have used a silicon JFET located within the cryostat (working at an operating temperature of T $\approx 150 \text{ K}$) as a high impedance input

stage which is then coupled to room temperature electronics, forming the remainder of the amplifier [13, 14, 15, 16]. Each JFET dissipates 5 mW of power which must be sunk by the cryostat. The typical achieved single channel charge resolution of $\sigma_E \approx .3 \text{ keV}_{ee}$ ¹ (100 electrons) sets a zero background low-mass detection threshold of roughly 10 GeV/c², preventing searches in the low-mass WIMP regime without the introduction of background events.

The CDMS and EDELWEISS collaborations have been investigating replacing the JFETs with high electron mobility transistors (HEMTs) recently developed by CNRS-LPN [17] specifically for readout of sub-Kelvin semiconductor detectors. The HEMTs have better noise performance, work natively at T $\leq 4 \text{ K}$, dissipate only 100 μW of power, and can have an input capacitance of 100 pF which is sufficiently well-matched to the typical detector capacitance. By replacing the JFET with a HEMT, we have already achieved equivalent charge resolution as the present CDMS JFET amplifier when coupled to a CDMS-II detector, with the room temperature electronics limiting the resolution [18]. Within the EDELWEISS collaboration, progress has been made using a voltage amplifier topology, however testing still needs to be performed with a live detector [19].

To maximize the performance advantages of switching to this new technology, we have developed a fully cryo-

*Corresponding author

Email address: arran@stanford.edu (A. Phipps)

¹keV_{ee} stands for keV-electron-equivalent, the amount of ionization energy produced by a 1 keV electronic recoil event.

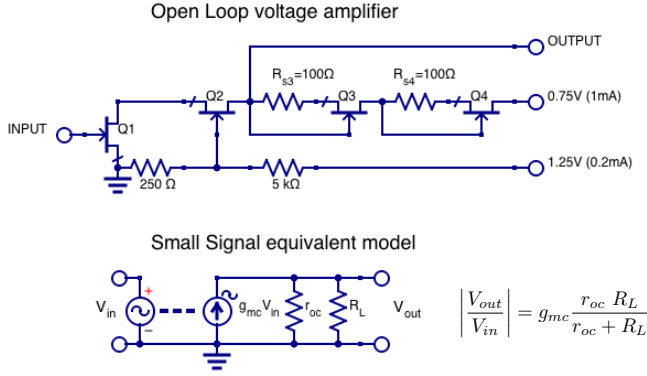


Figure 1: *Top* : The open loop voltage amplifier schematic. The HEMTs are labeled Q1-Q4. *Bottom* : The equivalent small signal model of the open loop amplifier.

Use in Amplifier	Q1	Q2, Q3, Q4
Device geometry	32 $\mu\text{m} \times 2 \text{ mm}$	4 $\mu\text{m} \times 5 \text{ mm}$
Power Dissipation	100 μW	100 μW
Transconductance g_m	36 mS	110 mS
Input Capacitance	100 pF	30 pF
Output Resistance r_o	1250 Ω	770 Ω
Noise @ 50 kHz	0.2 nV/ $\sqrt{\text{Hz}}$	0.2 nV/ $\sqrt{\text{Hz}}$
Noise @ 10 Hz	2.5 nV/ $\sqrt{\text{Hz}}$	5 nV/ $\sqrt{\text{Hz}}$

Table 1: Typical parameters of the two types of HEMTs used in the amplifier.

genic (T=4 K) charge amplifier constructed from multiple HEMTs. In this paper, we review the design and present the measured noise performance of the amplifier. We show an achieved optimal filter baseline energy resolution of $\sigma_E = 91 \text{ eV}_{ee}$ when coupled to a CDMS-II detector, verified by calibration with a radioactive source.

2. Open Loop Voltage Amplifier

The open loop design of the HEMT amplifier is shown in Fig. 1 and requires four HEMTs, labelled Q1-Q4. Two types of HEMT gate geometries are used to maximize performance. The amplifier is powered by two room-temperature voltage sources and dissipates a total power of 1 mW. The gate of Q1 should be held at a DC value of approximately -25 mV and can be adjusted to maximize gain. All components, other than the external power sources, are within the cryostat at the T=4 K layer.

The open loop amplifier takes a voltage signal present on the gate of Q1, which serves as the input port, and produces an inverted, amplified copy at the drain of Q2, which serves as the output port. Q1 and Q2 form a cascode, converting the input voltage into a current via the transconductance of Q1 with a boosted output impedance due to the addition of Q2, as seen in Eq. (1). The series impedance of the self-biased current sources Q3 and Q4 converts the signal current into the inverted, amplified output voltage at the Q2 drain. The cascode topology

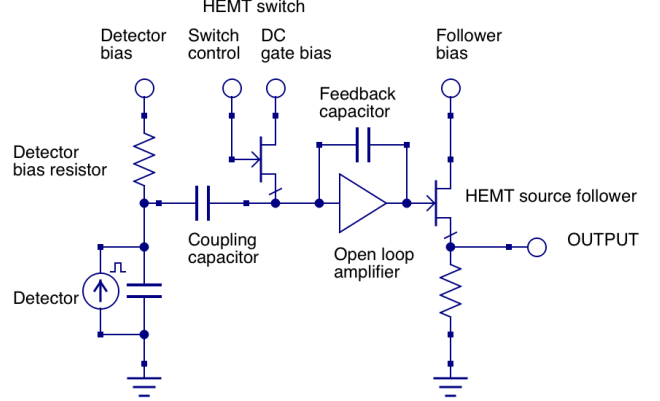


Figure 2: The closed loop amplifier. The triangle represents the open loop amplifier. A feedback capacitor closes the loop. A HEMT switch is added to reset the DC input voltage and is open during operation. A HEMT source follower is added to isolate the amplifier output from high capacitance cabling. The detector is AC-coupled to the input.

allows the current signal to be driven through the high active loads of Q3 and Q4, placed in series to increase the overall voltage gain [20].

The equivalent small signal model of the amplifier is also shown in Fig. 1, where g_{mc} is the cascode transconductance, r_{oc} the cascode output impedance, and R_L the total series impedance of the self-biasing current sources. With the typical single HEMT parameters of Table 1, the relevant HEMT amplifier parameter are given by:

$$\begin{aligned}
 r_{oc} &= r_{o1} + r_{o2} + g_{m2} \cdot r_{o1} \cdot r_{o2} \approx 108 \text{ k}\Omega \\
 g_{mc} &= \frac{g_{m1} \cdot r_{o1} \cdot (1 + g_{m2} \cdot r_{o2})}{r_{oc}} \approx g_{m1} \approx 36 \text{ mS} \\
 R_L &= r_{o3} + r_{o4} + R_{s3} + R_{s4} \\
 &\quad + g_{m3} \cdot r_{o3} \cdot R_{s3} + g_{m4} \cdot r_{o4} \cdot R_{s4} \approx 18 \text{ k}\Omega \\
 G_{ol} &= \left| \frac{V_{out}}{V_{in}} \right| = g_{mc} \frac{r_{oc} \cdot R_L}{r_{oc} + R_L} \approx 550
 \end{aligned} \tag{1}$$

The maximum achievable gain is $G_{ol} = g_{mc} \times r_{oc} \approx 3600$, which may be realized in the case that $R_L \gg r_{oc}$.

A prototype amplifier was constructed based on this design. The measured open loop gain was 340, limited by an effective load resistance of the Q3+Q4 combination of only $\sim 10 \text{ k}\Omega$. The smaller than expected measured load resistance is attributed to typical individual device variations, a common problem with open loop amplifiers. The -3dB bandwidth was 45 kHz, set by the stray capacitance of the cable ($\approx 100 \text{ pF}$) connecting the output to room temperature.

3. Closed Loop Charge Amplifier

The closed loop charge amplifier configuration is shown in Fig. 2. A small ($\approx 1 \text{ pF}$) capacitor is connected between the input and output to add feedback and stabi-

lize the gain. The detector is AC-coupled to the amplifier input through a 10 nF coupling capacitor. The total input capacitance C_{in} is the sum of the detector capacitance and HEMT input capacitance. The detector signal is a parallel current at the input, resulting in a voltage change (before considering amplifier and feedback effects) of $\Delta V_{in} = Q/(C_{in} + C_f)$ where Q is the total amount of charge generated in the detector by the interacting particle and C_f the feedback capacitance.

The closed loop voltage gain, taking into account the feedback and Miller effect, is given by:

$$G_{cl} = \frac{-G_{ol}}{1 + G_{ol} \cdot \beta} = \frac{-G_{ol}}{1 + G_{ol} \left(\frac{C_f}{C_{in} + C_f} \right)} \quad (2)$$

where G_{ol} is the open loop gain and $\beta = \frac{Z_{in}}{Z_{in} + Z_f}$ is the feedback factor [20]. If $G_{ol} \cdot \beta \gg 1$ and $C_{in} \gg C_f$, $\Delta V_{out} \approx -Q/C_f$. The closed loop gain only depends on the feedback capacitance and is not changed by variations in the open loop gain. As long as the open loop gain is high, the current at the input is simply integrated by the feedback capacitance. The change in voltage at the output ΔV_{out} thus provides an amplified measurement of the charge produced within the detector by an interacting particle.

In closed loop mode, a HEMT switch [21] is used to periodically reset the DC bias voltage at the amplifier input and remains open during data acquisition. When the switch is closed, the amplifier is placed into open loop mode. The switch HEMT has a small input capacitance of ≈ 5 pF to limit charge injection while switching and capacitive noise injection when open. A second low capacitance HEMT configured as a source follower isolates the output from room temperature cabling, adding an additional 100 μW of power dissipation. The follower lowers the overall gain by 8%, however the signal-to-noise is preserved and the amplifier bandwidth increased.

4. Standalone Noise Performance

To measure the noise performance, the amplifier input was first configured with a dummy detector capacitance of 180 pF, bringing the total input capacitance to ≈ 300 pF. Feedback was provided through 1.6 pF of capacitance (1 pF capacitor + 0.6 pF parasitic). For this measurement, no detector bias resistor was used in order to measure the intrinsic noise of the standalone amplifier. Although not required, a direct line from the output to room temperature which bypassed the follower was left connected, which limited the closed loop bandwidth to 80 kHz.

The closed loop voltage gain was measured using a small injection capacitor (not shown) and found to be $G_{ol} = 120$, in agreement with the full expression of Eq (2) when taking the limited open loop gain of $G_{cl} = 340$ into account. The HEMT switch transitioned from fully closed to fully open in $\approx 10 \mu s$. With the switch open, the input leakage current was measured to be $I_{leak} \leq 3 \cdot 10^{-17}$ A.

The output voltage noise power spectral density in open loop and closed loop mode was measured by both a Stanford Research Systems SR760 spectrum analyzer and a custom DAQ. The input equivalent voltage noise was determined by dividing the output noise by the measured gain and is shown in Fig. 3. In open loop mode, the measured noise is in good agreement with the typical intrinsic voltage noise of a single HEMT for the particular fabrication run used to produce the Q1 HEMT. The slight increase in our measured amplifier noise is believed to be due to individual HEMT variations.

In the closed loop mode, the total measured noise has contributions from both the intrinsic input HEMT voltage and current noises. While the intrinsic voltage noise e_n is the same for open and closed loop, the current noise i_n only contributes in the closed loop configuration and produces additional input voltage noise $Z_{in} \cdot i_n$ due to the total input impedance Z_{in} . This current noise is shunted by the switch in the open loop configuration. As the impedance of the input capacitance is inversely proportional to frequency, the closed loop noise increases at low frequencies.

A noise model based on best fits to the measured noise data gave the following input contributions:

$$\begin{aligned} e_{nTot} &= \sqrt{e_n^2 + (Z_{inTot} \cdot i_n)^2} \quad [\text{V}/\sqrt{\text{Hz}}], \\ i_n &= \sqrt{i_0^2 + a^2 \cdot f} \quad [\text{A}/\sqrt{\text{Hz}}] \quad \text{with} \\ Z_{inTot} &= 1/(2 \cdot \pi \cdot f \cdot (C_{in} + C_f)) \quad [\Omega], \\ e_n &= \sqrt{(0.23 \cdot 10^{-9})^2 + (10 \cdot 10^{-9}/\sqrt{f})^2} \quad [\text{V}/\sqrt{\text{Hz}}], \\ i_0 &= \sqrt{2 \cdot q \cdot I_{leak}} \quad [\text{A}/\sqrt{\text{Hz}}], \\ a &= 2 \cdot 10^{-17} \quad [\text{A}/\text{Hz}]. \end{aligned} \quad (3)$$

The measured noise is very close to the typical CNRS-LPN HEMT noise results already published [17, 21]. This implies that the total amplifier noise is completely dominated by the noise of the input HEMT Q1.

5. Predicted Charge Resolution from the Optimal Filter

As we know the detector response and the noise of the HEMT amplifier, the predicted charge resolution can be calculated using the optimal filter formalism [22]. The optimal filter performs a frequency-domain weighted least-square fit of a template shape to a measured signal pulse assuming the amplitude of the template scales linearly with the total charge. The RMS fluctuations σ_E (in keV_{ee}) of the fitted amplitude can be calculated by

$$\sigma_E^2 = \left(4 \int_{f_{min}}^{f_{max}} \frac{|s(f)|^2}{J(f)} df \right)^{-1} \rightarrow \left(4 \sum_{f_{min}}^{f_{max}} \frac{|s(f)|^2}{J(f)} \Delta f \right)^{-1} \quad (4)$$

where $s(f)$ is the frequency domain signal shape (the Fourier transform of the normalized 1 keV_{ee} time domain template shape), $J(f)$ is the single-sided noise power spectral

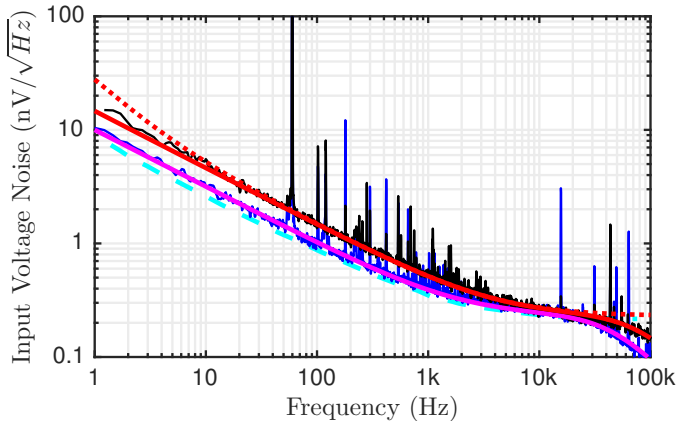


Figure 3: Input equivalent voltage noise of the HEMT amplifier. The measured open loop (blue) and closed loop noise (black) are compared with our model (Eq. 3) for e_n (magenta), $e_{nTot} = \sqrt{e_n^2 + (Z_{in} \cdot i_n)^2}$ (red). Also shown is the typical single HEMT voltage noise e_n from the same fabrication series as the Q1 HEMT (cyan, dashed). The red, dotted line shows the total input noise for the $C_{in} = 300$ pF, $R_{bias} = 2$ G Ω at $T = 20$ mK, $I_{leak} = 5$ fA configuration used in Table 2.

density (in V^2/Hz), and $f_{max} - f_{min}$ is the measurement bandwidth. In case of discrete sampling, the right hand side is used, where Δf is the spacing between measured frequencies.

The calculation is performed with respect to the amplifier input. The template shape is the equivalent input voltage generated by 1 keV of energy deposited in the detector in the form of electronic recoils. It takes 3 eV of energy for an electronic recoil to produce an electron-hole pair in sub-Kelvin germanium. A 1 keV energy deposition in the detector will thus create 333 electron-hole pairs. In the frequency domain the HEMT amplifier response is simply its total complex input impedance Z_{inTot} (Eq (3)), thus we define $s(f) = 333 \cdot e \cdot Z_{inTot}$, where e is the elementary charge in Coulomb.

In Table 2, we estimate the amplifier baseline energy resolution based on the expected total input capacitance of 300 pF for the upcoming SuperCDMS SNOLAB detectors [23] and present EDELWEISS detectors [14]. All noise sources are added in quadrature. The feedback capacitance is 1.6 pF for all configurations and has a negligible contribution to the total input impedance. The leakage current I_{leak} is taken to be 5 fA, much higher than the maximum 30 nA measured with the dummy detector, and is an upper limit of the maximum leakage current allowed on a detector without significantly degrading the resolution. The discrete case of Eq. (4) is used with the summation ranging from 10 Hz to 50 kHz in 1 Hz steps. In all cases we find an impressive $\sigma_E \approx 105$ eV $_{ee}$ resolution.

6. Performance with a CDMS Detector

To confirm the predicted resolution, a CDMS-II [1] germanium detector has been studied with the HEMT amplifier. The detector is 1 cm thick, 7.6 cm in diameter

C_{in}	R_{bias}	σ_E (eV $_{ee}$)
300 pF	No bias resistor	108
300 pF	2 G Ω at $T=20$ mK	109
240 pF	300 M Ω at $T=40$ mK	103

Table 2: Predicted optimal filter charge resolution σ_E in eV $_{ee}$ for various configurations using the HEMT amplifier noise model from Eq (3), with $I_{leak} = 5$ fA.

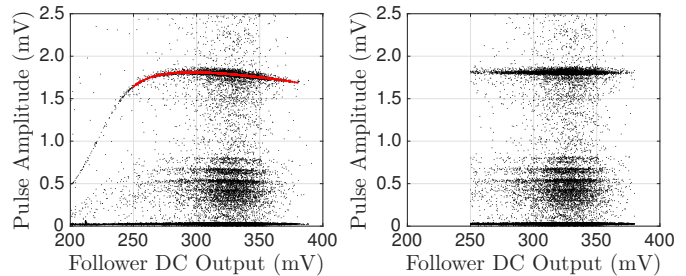


Figure 4: Pulse amplitude (in mV) of the ^{241}Am data vs HEMT amplifier DC output. *Left*: Uncorrected data. The red line shows the polynomial fit used to define the gain correction (see text). *Right*: After correction.

with a mass of ≈ 240 g. As the HEMT amplifier prototype has only one channel, the inner and outer electrodes were connected in parallel. The total capacitance of the detector is estimated to be 130 pF, resulting to a total input capacitance of 240 pF. The electrodes are polarized at 4.8 V through a bias resistor of 300 M Ω placed in close proximity to the detector. Both the bias resistor and detector are thermally sunk to the 40 mK base temperature stage of the cryostat. To have an unbiased measurement of the resolution, the detector response is studied with a collimated ^{241}Am source facing the detector. We have previously used this same setup to perform similar measurements [18]. From Table 2, the expected baseline energy resolution σ_E is at the 100 eV $_{ee}$ level.

We observed some variation of the closed loop gain (Eq 2) due to the relatively low open loop gain, which depends on the DC bias level at the input HEMT gate. To

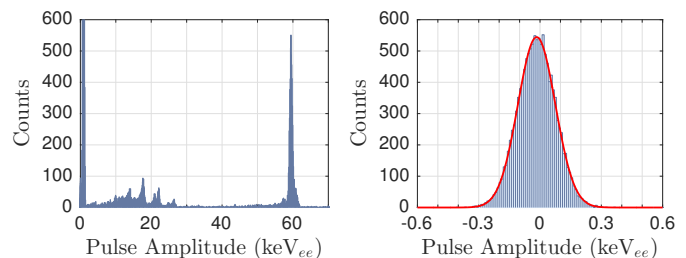


Figure 5: *Left*: Histogram of the ^{241}Am data in keV $_{ee}$, with a bin width of 0.1 keV $_{ee}$. The main lines of ^{241}Am L X-rays are 13.9, 17.8 and 20.8 keV and γ -rays are 26.4 and 59.5 keV. The RMS resolution deduced from a gaussian fit (not shown) to the 59.5 keV photopeak is 420 ± 15 eV $_{ee}$. *Right*: Histogram of a frequency domain optimal filter fit applied to a large number of baseline noise traces. The RMS baseline energy resolution deduced from a gaussian fit (red curve) is $\sigma_E = 91$ eV $_{ee}$.

correct this instability, both the DC and AC outputs of the follower were sampled at 200 kHz with a 16-bit ADC. An internal 5-pole Bessel filter at 100 kHz was used to prevent aliasing. As the follower DC output varies with the gate DC voltage of the input HEMT, the variation of the closed loop gain with the DC gate voltage can be monitored and corrected on an event-by-event basis. The left plot of Fig. 4 shows the uncorrected ^{241}Am photopeaks and their variations with the follower DC output. To define the gain correction, a 5^{th} order polynomial (red line) is fit to the 59.5 keV photopeak. A 0.25-0.38 V follower DC output selection cut is applied before the fit to reject outliers. Applying this energy-independent gain correction to the data set results in the right plot of Fig. 4.

The pulse amplitudes were found using the follower AC output by both a time domain fit and an optimal filter frequency domain fit. The photopeak positions and resolutions were the same for both methods. Fig. 4 and Fig. 5 (Left) were obtained with a 1 ms time window fit after application of a first order 100 Hz high pass filter. Fig. 5 (Left) is the histogram of the gain-corrected data shown in Fig. 4, calibrated to keV_{ee} based on the location of the 59.5 keV photopeak.

The 13.9, 17.8, 20.8, and 26.4 keV peaks are found at their expected locations, showing good linearity of the HEMT amplifier. The RMS resolution of the 59.5 keV peak is $420 \pm 15 \text{ eV}_{ee}$, very close to the resolution measured with the CDMS JFET amplifier (440 eV_{ee} RMS) [18]. The photopeak resolution is dominated by detector effects such as charge trapping [24, 25], explaining why the resolution is the same for both fitting methods and both amplifiers.

The baseline RMS energy resolution was found by applying the pulse fitting routine to a large number of baseline noise traces. In this case, the pulse start time must be held constant to prevent the fit from always finding the pulse amplitude to be the maximum noise fluctuation, which would produce a shifted non-Gaussian amplitude distribution and an incorrect result. As shown in Fig. 5 (Right), the frequency domain optimal filter obtained an RMS resolution of $\sigma_E = 91 \text{ eV}_{ee}$, compared to $\sigma_E = 130 \pm 1 \text{ eV}_{ee}$ when using the time domain fit (not shown). The measured resolution is $\approx 10\%$ better than the predictions of Table 2, possibly due to errors in the measured closed loop voltage gain or detector-related effects such as impact ionization [26], demonstrating the importance of using radioactive sources for an unbiased calibration. To our knowledge, this is the best baseline energy resolution achieved with such massive detectors of $\approx 150 \text{ pF}$ capacitance.

7. Conclusions

In conclusion, we have shown that sub-100 eV_{ee} baseline ionization resolution is achievable in massive dark matter detectors such as those used by the CDMS and EDELWEISS collaborations. The use of a CDMS-II detector in this work demonstrates the feasibility of this design

for future CDMS and EDELWEISS dark matter searches. Our fully cryogenic HEMT-based charge amplifier is a significant advancement over previous designs, allowing these experiments to improve their sensitivities to low-mass WIMPs ($\lesssim 10 \text{ GeV}/c^2$).

8. Acknowledgements

This work was supported in part by the National Science Foundation. We thank Matt Pyle, Xavier Defay and Nicholas Zobrist for their help and useful discussion in performing this work.

References

References

- [1] R. Abusaidi, et al., Exclusion limits on the WIMP-nucleon cross section from the Cryogenic Dark Matter Search, Phys. Rev. Lett. 84 (2000) 5699. doi:10.1103/PhysRevD.66.122003.
- [2] D. S. Akerib, et al., Exclusion limits on the WIMP-nucleon cross section from the first run of the Cryogenic Dark Matter Search in the Soudan Underground Laboratory, Phys. Rev. D 72 (2005) 052009. doi:10.1103/PhysRevD.72.052009.
- [3] Z. Ahmed, et al., Search for Weakly Interacting Massive Particles with the first five-tower data from the Cryogenic Dark Matter Search at the Soudan Underground Laboratory, Phys. Rev. Lett. 102 (2009) 011301. doi:10.1103/PhysRevLett.102.011301.
- [4] Z. Ahmed, et al., Dark matter search results from the CDMS II experiment, Science 327 (2010) 1619. doi:10.1126/science.1186112.
- [5] A. Juillard, et al., Status and prospects of the EDELWEISS-III direct WIMP search experiment, J. Low Temp. Phys. 184 (2016) 897. doi:10.1007/s10909-016-1493-0.
- [6] A. Armengaud, et al., Final results of the EDELWEISS-II WIMP search using a 4-kg array of cryogenic germanium detectors with interleaved electrodes, Phys. Lett. B 702 (2012) 329. doi:http://dx.doi.org/10.1016/j.physletb.2011.07.034.
- [7] A. Armengaud, et al., Search for low-mass WIMPs with EDELWEISS-II heat-and-ionization detectors, Phys. Rev. D 86 (2012) 051701. doi:10.1103/PhysRevD.86.051701.
- [8] A. Armengaud, et al., Constraints on low-mass WIMPs from the EDELWEISS-III dark matter search, Journal of Cosmology and Astroparticle Physics 05 (2016) 019. doi:10.1088/1475-7516/2016/05/019.
- [9] C. E. Aalseth, P. S. Barbeau, J. Colaresi, J. I. Collar, J. Diaz Leon, J. E. Fast, N. E. Fields, T. W. Hossbach, A. Knecht, M. S. Kos, M. G. Marino, H. S. Miley, M. L. Miller, J. L. Orrell, K. M. Yocum, CoGeNT: a search for low-mass dark matter using p -type point contact germanium detectors, Phys. Rev. D 88 (2013) 012002. doi:10.1103/PhysRevD.88.012002.
- [10] G. Angloher, et al., Results on low mass WIMPs using an upgraded CRESST-II detector, The European Physical Journal C 74 (12) (2014) 1–6. doi:10.1140/epjc/s10052-014-3184-9.
- [11] R. Agnese, et al., Search for low-mass Weakly Interacting Massive Particles with SuperCDMS, Phys. Rev. Lett. 112 (2014) 241302. doi:10.1103/PhysRevLett.112.241302.
- [12] R. Agnese, et al., Search for low-mass Weakly Interacting Massive Particles using voltage-assisted calorimetric ionization detection in the SuperCDMS experiment, Phys. Rev. Lett. 112 (2014) 041302. doi:10.1103/PhysRevLett.112.041302.
- [13] D. Akerib, et al., Design and performance of a modular low-radioactivity readout system for cryogenic detectors in the CDMS experiment, Nuclear Instruments and Methods in Physics Research A 591 (1998) 476. doi:10.1016/j.nima.2008.03.103.

- [14] B. Censier, et al., EDELWEISS read-out electronics and future prospects, *J. Low Temp. Phys.* 167 (2012) 645. doi:[10.1007/s10909-012-0568-9](https://doi.org/10.1007/s10909-012-0568-9).
- [15] E. Armengaud, et al., [Performance of the EDELWEISS-III experiment for direct dark matter searches](#), *Journal of Instrumentation* 12 (08) (2017) P08010. doi:[10.1088/1748-0221/12/08/P08010](https://doi.org/10.1088/1748-0221/12/08/P08010).
URL <http://stacks.iop.org/1748-0221/12/i=08/a=P08010>
- [16] A. T. J. Phipps, [Ionization Collection in Detectors of the Cryogenic Dark Matter Search](#), Ph.D. thesis, University of California, Berkeley (2016).
URL <http://lss.fnal.gov/archive/thesis/2000/fermilab-thesis-2016-36.pdf>
- [17] Q. Dong, et al., Ultra-low noise high electron mobility transistors for high-impedance and low-frequency deep cryogenic readout electronics, *Applied Physics Letters* 105 (2014) 013504. doi:[10.1063/1.4887368](https://doi.org/10.1063/1.4887368).
- [18] A. Phipps, et al., Ionization readout of CDMS detectors with low power, low noise HEMTs, *J. Low Temp. Phys.* 176 (2014) 470. doi:[10.1007/s10909-013-1062-8](https://doi.org/10.1007/s10909-013-1062-8).
- [19] X. de la Broise, et al., Cryogenic ultra-low noise HEMT amplifiers board, *Nuclear Instruments and Methods in Physics Research A* 787 (2015) 51. doi:<http://dx.doi.org/10.1016/j.nima.2014.11.016>.
- [20] P. R. Gray, P. Hurst, R. Meyer, S. Lewis, *Analysis and Design of Analog Integrated Circuits*, 4th edn., Wiley, 2001, Ch. 3, pp. 172–208.
- [21] Y. Jin, Q. Dong, A. Cavanna, U. Gennser, L. Couraud, C. Ulysse, Ultra-low noise hemts for deep cryogenic low-frequency and high-impedance readout electronics, in: *2014 12th IEEE International Conference on Solid-State and Integrated Circuit Technology (ICSICT)*, 2014, pp. 1–4. doi:[10.1109/ICSICT.2014.7021379](https://doi.org/10.1109/ICSICT.2014.7021379).
- [22] C. Enss, *Cryogenic Particle Detection.*, Springer-Verlag, Berlin Amsterdam, 2005, p. 17.
- [23] P. L. Brink, Conceptual design for SuperCDMS SNOLAB, *J. Low Temp. Phys.* 167 (5) (2012) 1093–1098. doi:[10.1007/s10909-011-0440-3](https://doi.org/10.1007/s10909-011-0440-3).
- [24] K. Sundqvist, A. Phipps, A. Dixit, B. Sadoulet, Transport and two-species capture of electrons and holes in ultrapure germanium at milliKelvin temperature, *J. Low Temp. Phys.* 176 (3-4) (2014) 188–193. doi:[10.1007/s10909-013-1064-6](https://doi.org/10.1007/s10909-013-1064-6).
- [25] M.-C. Piro, A. Broniatowski, S. Marnieros, L. Dumoulin, E. Olivieri, Hot carrier trapping in high-purity and doped germanium crystals at millikelvin temperatures, *J. Low Temp. Phys.* 176 (5-6) (2014) 796–801. doi:[10.1007/s10909-014-1088-6](https://doi.org/10.1007/s10909-014-1088-6).
- [26] A. Phipps, B. Sadoulet, K. M. Sundqvist, Observation of impact ionization of shallow states in sub-Kelvin, high-purity germanium, *J. Low Temp. Phys.* 184 (1) (2016) 336–343. doi:[10.1007/s10909-016-1472-5](https://doi.org/10.1007/s10909-016-1472-5).